Spontaneous ZnO nanowire formation during oxidation of Cu-Zn alloy

Lu Yuan, Chao Wang, Rongsheng Cai, Yiqian Wang, and Guangwen Zhou

CrossMark
click for updates

Spontaneous ZnO nanowire formation during oxidation of Cu-Zn alloy

Lu Yuan,[1] Chao Wang,[2] Rongsheng Cai,[2] Yiqian Wang,[2] and Guangwen Zhou[1,a)]
[1]*Department of Mechanical Engineering and Multidisciplinary Program in Materials Science and Engineering, State University of New York, Binghamton, New York 13902, USA*
[2]*The Cultivation Base for State Key Laboratory, Qingdao University, Qingdao 266071, China*

A combination of electron microscopy and *in-situ* x-ray diffraction is employed to study the thermal oxidation of brass ($Cu_{0.7}Zn_{0.3}$ alloy) in order to elucidate the mechanism of one-dimensional growth of ZnO nanostructures. Oxidation of the brass alloy results in the growth of a ZnO overlayer with ZnO nanowire formation on the ZnO layer. Increasing the oxidation temperature thickens the ZnO overlayer while suppressing ZnO nanowire formation on the top, which provides clear evidence that the formation of ZnO nanowires is related to a stress-driven mechanism that involves accumulation of compressive stress generated from the ZnO/Cu-Zn interfacial reaction and relaxation of the compressive stress by outward grain-boundary diffusion of Zn. © *2013 AIP Publishing LLC*. [http://dx.doi.org/10.1063/1.4812569]

I. INTRODUCTION

Zinc oxide (ZnO), a semiconductor with a direct wide band gap (3.37 eV) and large exciton binding energy (60 meV), has received extensive interest due to its wide potential applications in electronics, optics, and photonics.[1–3] ZnO also exhibits a diversity of nanostructures and morphologies including wires,[4] belts,[2] tubes,[5] rods,[6] springs,[7] and rings.[8] One-dimensional (1D) ZnO is expected to open wide-ranging application possibilities ranging from nanophotonics, nanoeclectronics to nanobiotechnology.[9–12] Various methods such as vapor-solid (VS), vapor-liquid-solid (VLS), epitaxial growth, hydrothermal, and other solution processes have been used to produce 1D ZnO entities.[13–15] Compared to these methods, thermal oxidation of metallic zinc is a simple approach to generate 1D ZnO nanostructures with the large-scale growth capabilities. The oxide nanostructures obtained by this approach show high purity since it eliminates the need for multistage processes of catalytic chemical synthesis of oxide nanostructures that involve many intermediaries.

ZnO nanostructures have been obtained by directly heating Zn substrates in air or an oxygen containing atmosphere.[3,16] Since the melting temperature of zinc is relatively low (419.5 °C), oxidation of Zn at high temperatures usually results in highly roughened surfaces. To overcome this issue, oxidation of Zn thin films on substrates, such as Si,[17] CdTe,[18] and sapphire[19] with a ZnO buffer layer, has been pursued to produce 1D ZnO nanostructures.[20,21] However, the thermal expansion coefficient differences between the ZnO buffer layer and the substrates usually cause deleterious effect on their interfacial adhesion. Additionally, the poor conductivity of these substrates might limit the applications of ZnO nanostructures in electronics and optoelectronics.[22] It was recently showed that ZnO nanowires can grow on brass (Cu-Zn alloy) substrates by directly oxidizing brass in an oxygen atmosphere.[22–24] Brass with a Zn content less than 35% stays as a solid at the temperature up to 900 °C,[25]

which is beneficial for the formation and applications of ZnO nanostructures at high temperatures. For ZnO nanowire formation from thermal oxidation of pure zinc that typically involves liquid and/or vapor phase of Zn due to the high oxidation temperatures employed to promote the oxide nanostructure formation, the VS mechanism is usually invoked to understand the oxide growth morphologies.[18,26] However, ZnO nanowire growth from oxidation of Cu-Zn does not involve liquid or vapor phase due to the high melting point of Cu-Zn. This suggests a completely different growth mechanism governing the formation of ZnO nanowires during the oxidation of brass, but it has not yet been addressed.

In this work, we present a detailed study on the formation of ZnO nanowires during the oxidation of brass at high temperatures. Particularly, the effect of oxidation temperature on the oxide growth morphology has been examined in detail in order to elucidate the mechanism underlying the formation of ZnO nanowires. In contrast to the oxidation of pure zinc, where a higher temperature promotes ZnO nanowire growth,[27,28] we find that increasing the oxidation temperature actually suppresses the formation of ZnO nanowires. This result demonstrates a stress-driven mechanism leading to the formation of ZnO nanowire formation, which is fundamentally different from the proposed VS process for ZnO nanowire formation from the oxidation of pure Zn.

II. EXPERIMENTAL

High-purity brass ($Cu_{0.7}Zn_{0.3}$ alloy) substrates (99.98%) with a thickness of 0.25 mm are used in the oxidation experiments. The brass substrate is textured polycrystalline as examined by x-ray diffraction (XRD). The brass sheets are cut into approximately 1 cm × 1 cm foils and then thoroughly rinsed with deionized water followed by ultrasonication in acetone for 5 min. The cleaned brass substrates are dried in N_2 and then placed on a substrate heater in a vacuum chamber and the sample temperature is monitored using a K-type thermocouple in contact with the substrate heater. The oxidation chamber is first pumped to vacuum ($\sim 2 \times 10^{-6}$ Torr), and then filled with oxygen gas at the pressure of 300 mbar

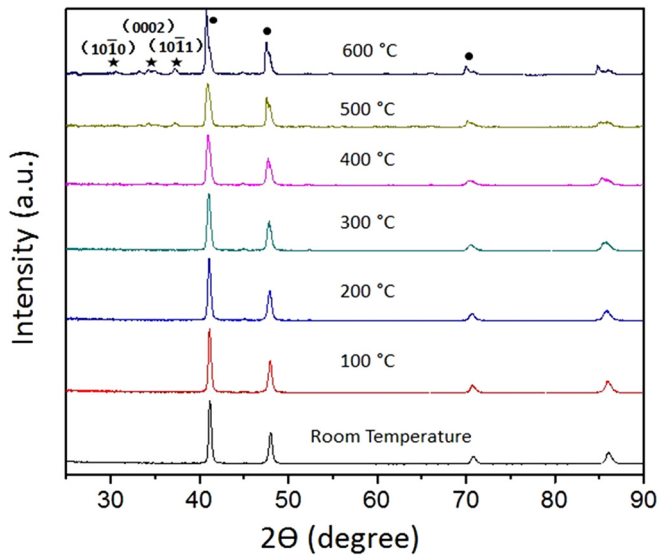a)Author to whom correspondence should be addressed. E-mail: gzhou@binghamton.edu

FIG. 1. *In situ* X-ray diffraction patterns obtained at different temperatures for $Cu_{0.7}Zn_{0.3}$ foil during the heating process in air with a heating rate of 20 °C/min. The scan for each XRD pattern takes ~15 min to complete.

(oxygen purity is 99.999%). The chamber is then sealed and the brass samples are heated to 300 °C ~ 600 °C at a rate of ~20 °C/min and oxidized at the temperature for different durations. It is then cooled down in the same oxygen atmosphere to room temperature at a rate of ~10 °C/min. Growth morphology and chemical composition of the oxidized samples are examined using field emission scanning electron microscopy (FEG-SEM, FEI Supra 55VP) and energy-dispersive X-ray spectroscopy (EDS). *In situ* X-ray diffraction (XRD, PANalytical's X'Pert) is used to monitor the formation of ZnO during the oxidation of brass. The thickness of the oxide layer formed from the oxidation is measured from cross-sectional SEM samples prepared by a cross

section polisher. Grain structures in the oxide layers are examined by fractured cross sections of the samples. Cross-sectional transmission electron microscope (TEM) specimens are made from the brass foils oxidized at 300 °C. The microstructures of nanowires are analyzed using a JEOL JEM 2100 F TEM operated at 200 kV.

III. EXPERIMENTAL RESULTS

In situ XRD was employed to monitor the formation of different possible oxide phases during the heating process of the oxidation. Fig. 1 shows *in situ* XRD results of the $Cu_{0.7}Zn_{0.3}$ foil during heating process in air at the heating rate of 20 °C/min. It can be seen that from room temperature to 400 °C, there only shows peaks of the Cu-Zn alloy. The peaks of ZnO start to show up at 500 °C and become stronger at 600 °C. It can be seen that there are no peaks of CuO or Cu_2O found in these XRD patterns, suggesting that Cu is not oxidized during the heating process. This is because Cu is more noble than Zn, and even if there is little CuO formed, it may be easily reduced to Cu by $Zn + CuO = ZnO + Cu$ since ZnO is thermodynamically more stable than CuO under the oxidation condition. The peaks associated with the Cu-Zn alloy shift slightly to the low-angle side with increasing the oxidation temperature due to the thermal expansion effect.

To examine the oxide growth morphologies, brass foils are oxidized in pure oxygen at different temperatures. Fig. 2 shows typical SEM images obtained from the samples oxidized at the oxygen pressure of 300 mbar for 1 h. As can be seen in Fig. 2(a), at the relatively low oxidation temperature (300 °C), the surface is covered by dense nanowires, with diameters of ~30 nm and length up to microns. Figs. 2(b)–2(f) show representative SEM images obtained from the samples oxidized at 350 °C, 400 °C, 450 °C, 500 °C, and 600 °C, respectively. As can be seen clearly, with increasing
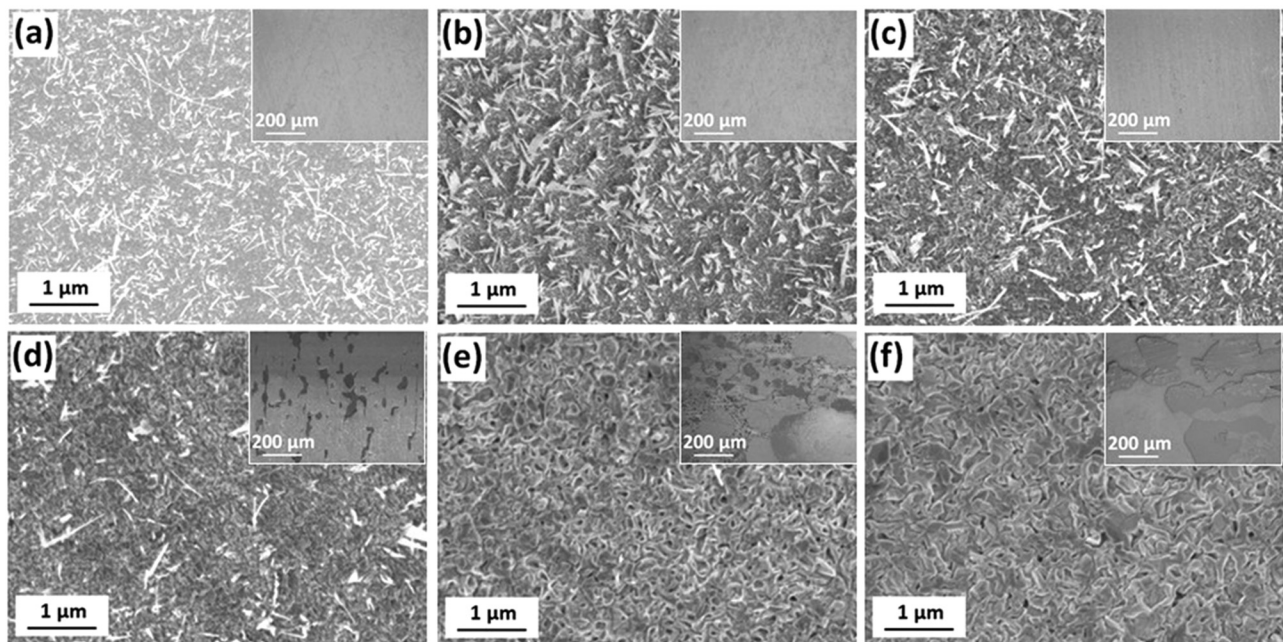

FIG. 2. Typical SEM images of the brass substrates oxidized at different temperatures under the oxygen pressure of 300 mbar. (a) 300 °C; (b) 350 °C; (c) 400 °C; (d) 450 °C; (e) 500 °C; and (f) 600 °C. Insets are corresponding SEM images showing the low-magnification overview of the surface.

the oxidation temperature, the surface density of nanowires decreases gradually. There are few nanowires formed at 500 °C (Fig. 2(e)) and no nanowires are observed on the surface oxidized at 600 °C (Fig. 2(f)). SEM examination also reveals that the surfaces of the oxidized samples start to form cracks for the oxidation temperatures at 450 °C and above. As can be seen from the inset SEM images in Fig. 2, the overview of the low-magnification surface morphology shows that the surface of the brass sample oxidized at 350 °C is still smooth; however, some cracks are visible on the samples oxidized at 450 °C. The oxide layers form more and larger cracks, and part of the oxide layer peels off from the brass substrates for the oxidation at 500 °C and 600 °C.

Fig. 3 illustrates XRD patterns obtained *ex situ* from the above samples shown in Fig. 2. It can be seen that all the peaks are composed of Cu-Zn and hexagonal wurtzite ZnO. The peak intensity of the ZnO phase formed from the oxidation at 300 °C is weak, suggesting that the ZnO layer is very thin (as confirmed by cross-sectional SEM images shown in Fig. 7) although it shows the highest density of ZnO nanowires. Compared with the *in situ* XRD data (Fig. 1) obtained from the oxidation in air, where ZnO peaks start to show up at temperatures around 500 °C and above, it can be seen that a higher oxygen pressure can promote ZnO formation even at a much lower oxidation temperature. The intensity of the ZnO peaks become stronger for the samples oxidized at the higher temperatures, suggesting that the thickness of the ZnO layer increases with increasing the oxidation temperature. Similarly, there are no peaks showing the formation of CuO, consistent with the *in situ* XRD experiments. Compared to the XRD data shown in Fig. 1, the *ex situ* XRD data in Fig. 3 were obtained from the Cu-Zn samples that were oxidized isothermally in pure oxygen with a higher oxygen partial pressure (compared to air) and a longer oxidation duration. By combing the results in Figs. 2 and 3, it can be seen that while increasing the oxygen pressure and/or oxidation time promotes the selective oxidation of Zn in the alloy (still not Cu oxide formation), it does not necessarily leads to the growth of more ZnO nanowires.
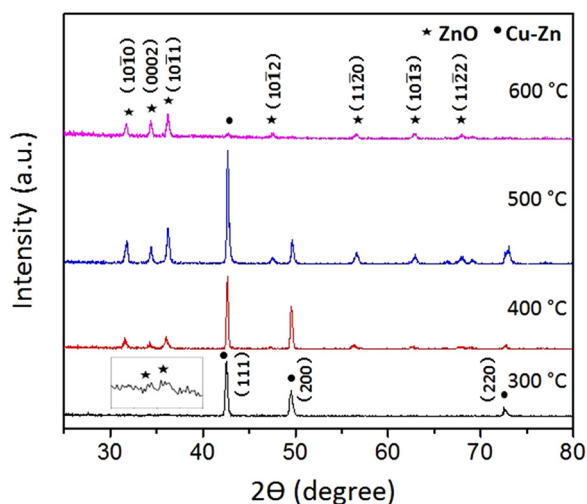

FIG. 3. Room temperature XRD patterns obtained from the brass substrates oxidized for 1 h at the different temperatures under the oxygen pressure of 300 mbar.

However, different from the *in situ* XRD pattern shown in Fig. 1, where all the peaks associated with Cu-Zn show a systematic shift toward lower diffraction angles gradually due to the thermal expansion effect with increasing the oxidation temperature, careful examination of the XRD pattern in Fig. 3 reveals that the peaks of the Cu-Zn alloy shift to higher diffraction angles for the samples oxidized at a higher temperature. The trend is particularly conspicuous for the (220) peak (i.e., around $2\theta = 73°$). Since the oxidation at the higher temperature results in more ZnO formation for a fixed period of the oxidation time, the systematic peak shift suggests that the lattice constant of the Cu-Zn alloy decreases with the increased ZnO formation. The XRD patterns in Fig. 3 were obtained at room temperature and no thermal expansion effect is thus involved. The shifting of the Cu-Zn peaks to higher angles can be attributed to the gradual consumption of Zn in the Cu-Zn alloy for ZnO formation during the oxidation, which correspondingly results in the enrichment of Cu in the Cu-Zn alloy. This corroborates with the earlier studies, which showed that the lattice constant of Cu-Zn alloys decreases with increasing Cu composition in the alloy.[29,30]

The thickness of the oxide layers is examined by cross-sectional SEM images. Fig. 4 shows representative cross-sectional SEM images of the brass samples oxidized for 1 h at 300 °C, 350 °C, 400 °C, 450 °C, 500 °C, and 600 °C, respectively. It can be seen that the oxidation results in the growth of a single ZnO layer located directly above the Cu-Zn substrate and ZnO nanowire formation on the ZnO layer. The oxide nanowires are relatively aligned and perpendicular to the substrate surface. A clear trend noted from the cross-sectional SEM images is that with increasing the oxidation temperature, the thickness of the ZnO oxide layer increases while the surface density of ZnO nanowires decreases. There is no nanowire formation at the oxidation temperature of 600 °C that gives the largest thickness of the ZnO layer. Fig. 5 shows the dependence of the surface density of ZnO nanowires on oxidation temperature and thickness of the underlying ZnO layer, which reveals clearly that the formation of ZnO nanowires is gradually suppressed with increasing the oxidation temperature and the thickening of the underlying ZnO layer.

Cross-sectional TEM specimens are made from the oxidized samples to examine the ZnO/Cu-Zn interface region and ZnO root areas. Fig. 6(a) shows a typical cross-sectional TEM image of a brass substrate oxidized at 300 °C, which reveals clearly that it is a three-layered structure. It can be seen that the oxidation results in a single ZnO layer on the Cu-Zn alloy and the thickness of the ZnO layer is ~250 nm, consistent with the cross-sectional SEM results as shown in Fig. 4. It can be also noted from Fig. 6(a) that ZnO nanowires form and grow on top of underlying ZnO grains, which appears as grain protrusion on the ZnO layer (grain boundaries are not readily distinguishable in the TEM image, but the grain feature can be easy to resolve in the cross-sectional TEM images shown later in Fig. 7). Fig. 6(a) also shows that ZnO nanowires have a tapered shape with a larger diameter at the base. Fig. 6(b) displays a HRTEM image form the interface region between the ZnO overlayer and the Cu-Zn substrate, which shows their epitaxial relationship: $\{0002\}_{ZnO} // \{110\}_{Cu-Zn}$. However, it can
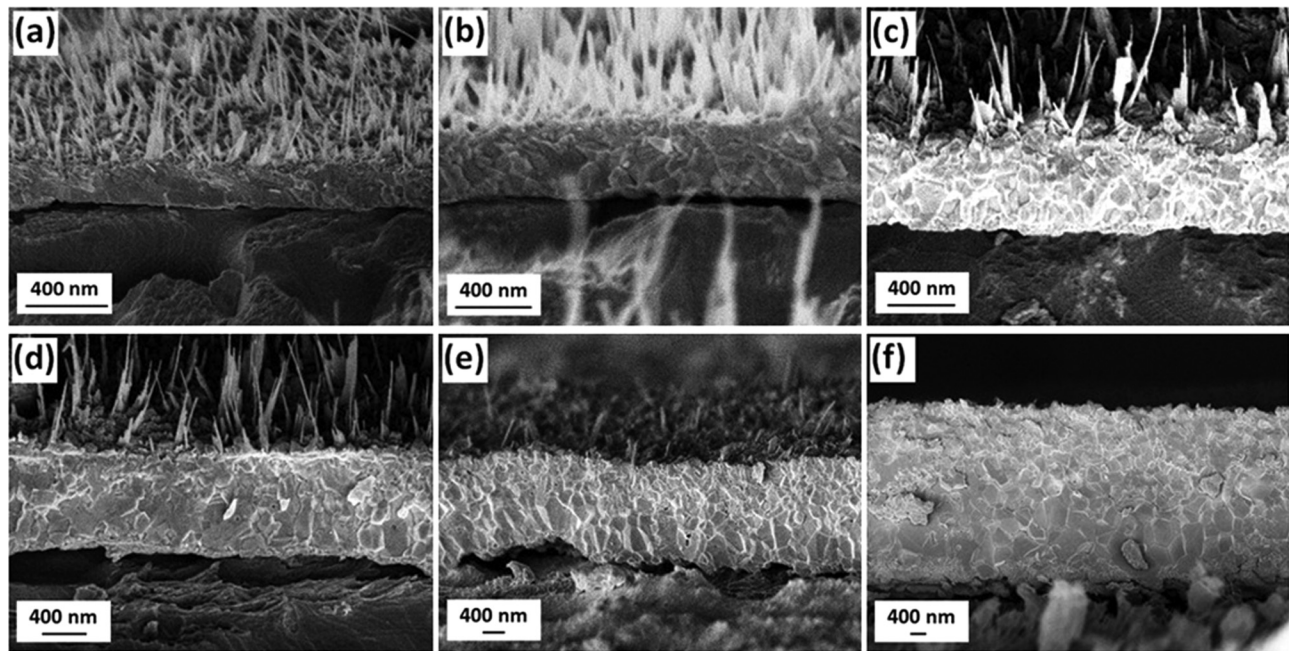
FIG. 4. Cross-sectional SEM images of the brass substrates oxidized for 1 h under the oxygen pressure of 300 mbar and the oxidation temperature of (a) 300 °C; (b) 350 °C; (c) 400 °C, (d) 450 °C; (e) 500 °C; and (f) 600 °C.

be seen that misfit dislocations occur at the interface, suggesting the existence of interfacial lattice strain. Fig. 6(c) shows an HRTEM image and typical SAED pattern (inset) obtained from the Cu-Zn region, which reveal that the underlying brass grain is a single crystal with a cubic structure. The crystalline nature and microstructure of ZnO nanowires is also examined by HRTEM and Fig. 6(d) shows a typical HRTEM image obtained from a single nanowire, which reveals that the nanowire has a bi-crystal structure with the twin boundary in middle along the nanowire axial direction.

To identify the growth roots at the substrate, the brass sample was oxidized for a shorter duration to reveal the initial growth morphology of ZnO nanowires. Fig. 7(a) shows an overall view of the initial growth of nanowires, it can be seen that the oxidized surface consists of faceted ZnO grains and nanowires form directly on top of the grains. Figs. 7(b)–7(d) show the different growth stages of individual
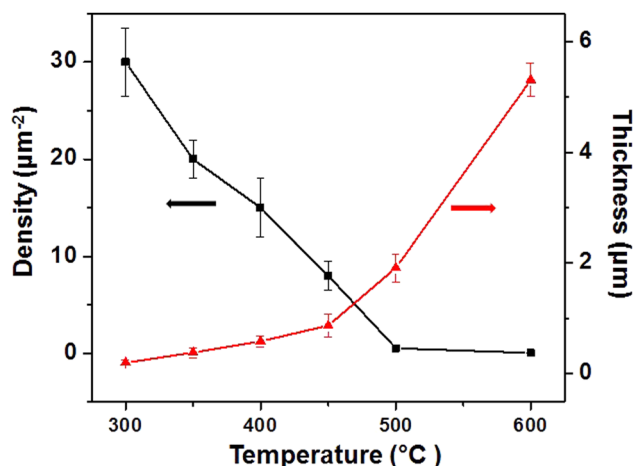
nanowires (not from the same nanowire) for their different lengths and reveal the growth of ZnO nanowires on the top of underlying ZnO grains rather than from grain boundary areas. Fig. 7(e) is a cross-sectional TEM view of ZnO nanowire growth, which further confirms that the nanowire grows on top of the ZnO grain.

We examined a large number of ZnO nanowires using HRTEM imaging and noted that almost all the nanowires exhibit the same bi-crystal structure. While the locations of the

FIG. 5. Dependence of the surface density of ZnO nanowires and thickness of the underlying ZnO layer on the oxidation temperature.
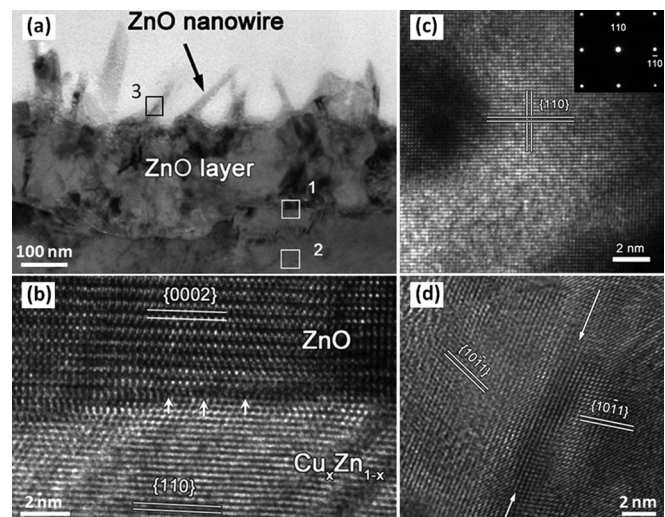

FIG. 6. (a) Cross-sectional BF TEM image showing three-layered structure: from top to bottom are ZnO nanowires, ZnO oxide layer, and Cu-Zn substrate; (b) HRTEM image of the ZnO/Cu-Zn interface corresponding to the marked rectangle area (1) in (a), white arrows show the locations of misfit dislocations, slight lattice distortion in the interface region can be also discerned; (c) HRTEM image obtained from the marked rectangle area (2) in (a), inset is a SAED pattern from the Cu-Zn layer, which shows a [001] zone axis; (d) HRTEM image recorded from the rectangle area (3) of a ZnO nanowire in (a) showing the existence of a twin boundary along the length direction of the nanowire.
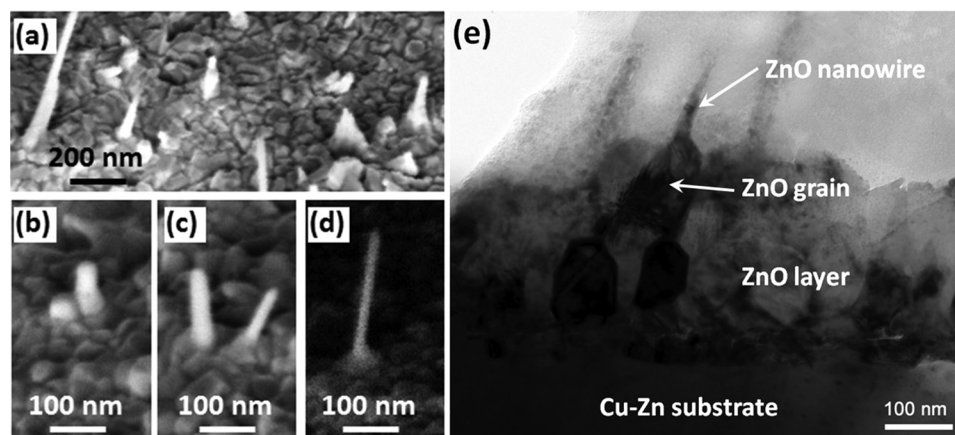
FIG. 7. (a) SEM micrograph of a brass substrate oxidized at 400 °C for ~20 min, showing the initial growth morphology of the ZnO nanowires; (b)–(d): SEM images of the different growth stages of individual ZnO nanowires; (e) cross-sectional BF TEM image showing the nanowire root region and the underlying ZnO grain.

bi-crystal boundary may vary for different nanowires, the two sides of the bi-crystal nanowires have the same type of the lattice planes $\{10\bar{1}1\}$, as shown in Fig. 6(d). Since ZnO nanowires grow directly on top of underlying ZnO grains, where the ZnO grains serve as the structure template for initiating ZnO nanowire growth, the typically observed lattice planes of $\{10\bar{1}1\}$ in the nanowires suggest that the exposed surfaces of the underlying ZnO grains are dominated by $\{10\bar{1}1\}$. This is very likely since the $\{10\bar{1}1\}$ facet has the lowest surface energy compared to other ZnO surfaces.[31] The brass substrate is textured polycrystalline, and the ZnO layer formed from the oxidation is polycrystalline in nature. The orientation of the exposed $\{10\bar{1}1\}$ surfaces depends on the orientation of the ZnO grains in the ZnO layer, which thus puts stipulation on the orientation (e.g., perpendicular or inclined with the substrate) of ZnO nanowires. As seen in Fig. 7(e), a tilt ZnO grain leads to the growth of a ZnO nanowire that is inclined with the substrate surface.

IV. DISCUSSION

Brass with a Zn content less than 35% (as our case $Cu_{0.7}Zn_{0.3}$) stays as a solid at the temperature up to 900 °C.[25] While the data regarding the vapor pressure of Zn in Cu-Zn is not readily available in the literature, its high melting point suggests a much lower vapor pressure for brass compared to pure Zn. In addition, the formation of an underlying ZnO layer on the brass substrate can prevent Zn evaporation (if any) from the brass surface. Thus, the ZnO nanowire formation is mostly related to the solid-state diffusion of Zn from the brass substrate through the ZnO layer to the outer surface. A clear trend revealed from the oxidation of the Cu-Zn alloy described above is that the surface density of ZnO nanowires decreases with increasing the oxidation temperature and nanowire formation is completely suppressed at the oxidation temperature of 600 °C. This is in sharp contrast to the oxidation of pure Zn, where ZnO nanowire formation is promoted by increasing the oxidation temperature.[30] Meanwhile, the thickness of the ZnO layer increases from 200 nm to 5.3 μm with increasing the oxidation temperature from 300 °C to 600 °C. The oxidation temperature at 300 °C has the thinnest thickness of the underlying ZnO layer but the highest surface density of ZnO nanowires. Apparently, the surface density of ZnO nanowires is correlated to the

thickness of the ZnO layer, i.e., the nanowire surface density decreases with the increase in the thickness of the underlying ZnO layer.

Because Zn has higher oxygen affinity than Cu, Zn species will diffuse along grain boundaries in the brass to the surface and then react with oxygen during the oxidation, forming a ZnO oxide layer on the surface. Growth stress will be generated at the ZnO/Cu-Zn interface due to the volume differences between the oxide formed and the metal consumed, which can be described as Pilling–Bedworth ratio (PBR), $PBR = \frac{volume\ of\ formed\ oxide}{volume\ of\ consumed\ metal}$.[32] In our experiments, Zn in the Cu-Zn alloy is selectively oxidized to form ZnO and the PBR is 1.58 for oxidation of Zn, i.e., the volume of the oxide formed is larger than that of the metal consumed. Their mole volume mismatch will generate compressive stress in the ZnO layer, particularly in the inner part adjacent to the ZnO/Cu-Zn interface. The stress can be usually released by the different responses, such as cracking of the oxide, spalling of the oxide from the alloy substrate, plastic deformation of the metallic substrate, and plastic deformation of the oxide.[32]

In addition to the stress relaxation mechanisms mentioned above, we recently proposed that compressive stresses accumulated in the oxide layer can be released by oxide nanowire growth.[33–36] In this mechanism, the compressive stress generated by the volume change accompanying the interfacial reaction during layered oxide growth stimulates oxide nanowire formation. The observed ZnO nanowire formation during the brass oxidation can be explained similarly and satisfactorily by the stress-driven mechanism. The stress driving the formation of ZnO oxide nanowires originates from the molar volume mismatch at the ZnO/Cu-Zn interface. The ZnO layer adjacent to the interface is under compression exerted by the Cu-Zn substrate due to its smaller molar volume, while the outer surface of the ZnO layer is stress free. Therefore, a stress gradient exists across the ZnO layer and drives the outward diffusion of Zn ions from the high stress region of the ZnO/Cu-Zn interface through grain boundaries in the ZnO layer to the low stress region of the outer surface, where Zn ions are deposited and then react with impinging oxygen molecules to form ZnO. The formation of bi-crystal structure in ZnO nanowires suggests that nanowires nucleate on top of exposed ZnO grains and the crystals grown on the adjacent surfaces of a single ZnO grain are joined to form a
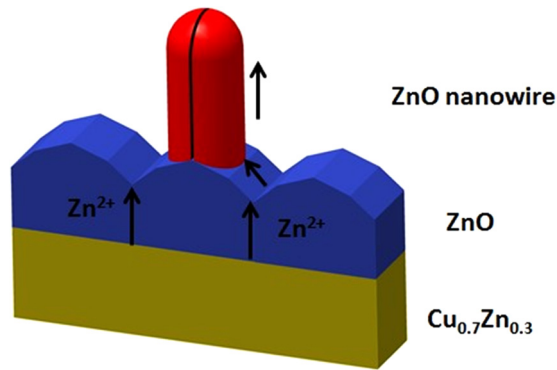
FIG. 8. Schematic illustration of the growth process of a single ZnO nanowire: Zn ions diffuse outward from the ZnO/Cu-Zn interface to the free surface via grain boundary diffusion driven by the ZnO/Cu-Zn interfacial reaction, followed by surface diffusion to the nanowire root and then to the nanowire tip driven by the concentration gradient.

twin structure with the twin boundary started from the grain top and continued into the nanowire along its growth direction. Fig. 8 shows schematically the growth process of a single ZnO nanowire by this mechanism.

Based on the mechanism described in Fig. 8, it is possible to form higher-order (e.g., triple, quadrupole) twin boundaries in nanowires if the underlying ZnO grains exhibit multiple facets. However, experimentally, we only observed two-dimensional bi-crystal nanowires. Two reasons may contribute to this discrepancy. First, as described above, the exposed surfaces of the ZnO grains are dominated by the $\{10\bar{1}1\}$ facet due to its smallest surface energy compared to other facets, thus the formation of bi-crystal nanowires with the side planes $\{10\bar{1}1\}$ is both kinetically and energetically more favorable than that of higher-order twin boundary nanowires that may exhibit high surface energy facets. Second, there may be high-order twin boundary nanowires but experimentally we were not able to resolve because of the nature of the TEM two-dimensional projection view of the three-dimensional structure of the nanowires.

For the stress-driven mechanism to be operative effectively, the underlying oxide layer should be sufficiently thin. For instance, our earlier experiments on the oxidation of Cu and Fe showed that the thickness of the top oxide layer (CuO or Fe_2O_3) is less than $1\,\mu m$ for CuO or Fe_2O_3 nanowire formation.[32–34] Otherwise, the stress will be released by other mechanisms such as cracking and spalling of the oxide layer and/or plastic deformation of the oxide and metal

substrate if a thick oxide scale develops. From the brass oxidation at the different temperatures, we observed that ZnO nanowire formation occurs only on the relatively thin ZnO layer at the temperature range of 300 °C to 450 °C, where the thickness of the underlying ZnO layers on the brass substrate varies from $0.2\,\mu m$ to $0.875\,\mu m$ (see Fig. 4). For the oxidation at 500 °C, the thickness of the ZnO layer is $\sim 2\,\mu m$ and there are barely ZnO nanowires on the surface. The oxidation at 600 °C results in a thick ZnO layer ($\sim 5.3\,\mu m$) and ZnO nanowire formation is thus completely suppressed. Alternatively, the growth stresses for the growth of such thick oxide scale are released by oxide cracking and spallation. This can be evidenced from the low-magnification overviews of the surface morphologies of the oxidized brass samples (Fig. 2), which demonstrate that the brass surfaces are flat for the oxidation at the lower temperatures while significant oxide cracking and spallation are observed from the oxidation at 600 °C.

To confirm the correlation between ZnO nanowire formation and thickness of the ZnO layer described above, we also examine the effect of oxidation time on the oxide nanowire growth. Fig. 9 shows SEM images obtained from a brass sample oxidized at 300 °C and oxygen pressure of 300 mbar for 3 h. From Fig. 9(a), it reveals that the surface density of the nanowires is higher than that for the oxidation for 1 h (see Fig. 2(a)). Fig. 9(b) shows a cross-sectional SEM image of the oxidized brass sample (note that the cross-sectional SEM sample was made by a cross section polisher, which preserves the interface structure and has much less damage due to the use of an argon ion beam). The thickness of the ZnO layer is $\sim 200\,nm$, very close to the thickness of the oxide layer formed from the oxidation at 300 °C for 1 h. It is interesting to note that the extended oxidation time actually promotes ZnO nanowire formation (i.e., longer length and high surface density) rather than for growing a thicker ZnO layer. This can be attributed to the thin thickness of the oxide layer that allows for efficient relaxation of the interfacial stress for ZnO growth rather than the thickening of the oxide layer that will hinder nanowire formation.

Further insight into the nanowire formation mechanism is obtained by the oxidation at higher temperatures but with shorter periods. Fig. 10 shows the oxidation at 500 °C and oxygen pressure of 300 mbar with the oxidation duration varying from 5 min to 45 min. Figs. 10(a) and 10(b) show representative planar and cross-sectional SEM images of the brass sample oxidized for 5 min. Very few nanowires are
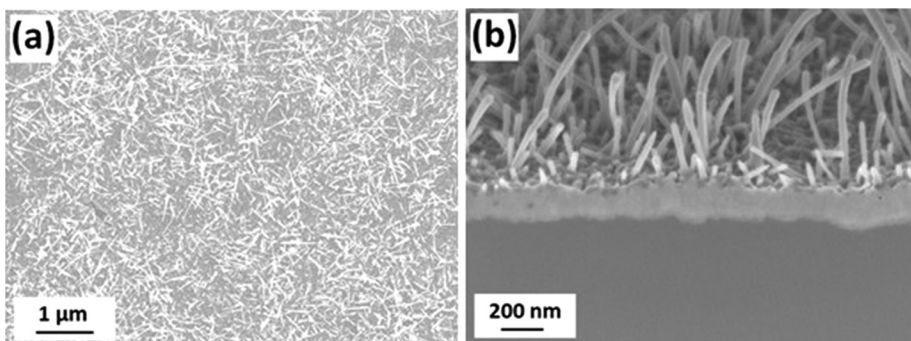

FIG. 9. Surface and interface SEM images of brass foil oxidized in oxygen at 300 °C for 3 h.
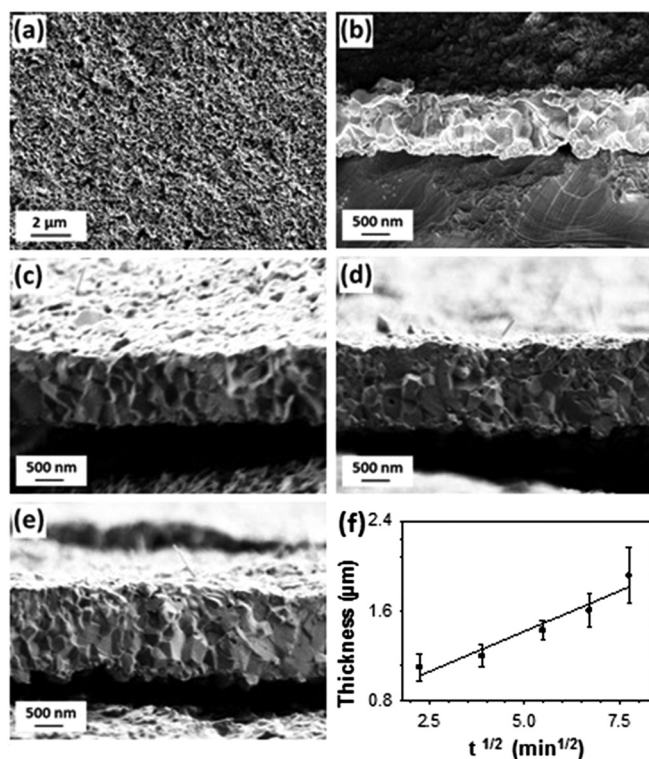
FIG. 10. (a) Surface morphology of the brass oxidized in oxygen at 500 °C for 5 min; (b)–(e) Cross-sectional SEM images of the brass oxidized for 5 min, 15 min, 30 min, and 45 min, respectively; (f) oxide thickness vs. square root of oxidation time.

observed across the entire surface, and the cross-sectional SEM image reveals that the thickness of the ZnO layer is already ~1.1 μm for such a short period of the oxidation. Figs. 10(c)–10(e) are interfacial SEM images of the brass samples oxidized for 15, 30, and 45 min, respectively, which shows evidently that there is barely nanowire formation for the different oxidation duration; however, the ZnO layer thickens with increasing the oxidation time.

As noted from above, ZnO nanowire growth requires effective grain boundary diffusion driven by the compressive stress. With increasing the oxidation temperature, lattice diffusion is also enhanced and may become comparable to the grain boundary diffusion. The observation shown in Fig. 10 suggests that the oxidation at 500 °C has led to significant lattice diffusion, resulting in uniform oxide growth and thus flatter surface morphologies at the high temperature. For oxide thickening controlled by bulk diffusion, oxide growth should follow the parabolic growth law, i.e., $x \sim (2kt)^{1/2}$, where x is the thickness of the oxide layer, k is the rate constant, and t is the oxidation time.[32] Parabolic plot of the oxide layer thickness thus yields a straight line. Fig. 10(f) shows the measured thickness of the ZnO layer vs. the square root of oxidation time, which shows a relatively straight line and confirms that the growth of the ZnO layer is a result of outward diffusion of Zn cations through the oxide layer[37] and the Zn cations supplied from the Cu-Zn substrate are completely incorporated into the ZnO oxide layer. This is different from the oxidation at the lower temperatures (e.g., 300 °C), for which a portion of the Zn ions supplied from the grain boundary diffusion are incorporated into ZnO nanowire

growth. The rapid growth of the oxide layer by lattice diffusion at the high temperatures results in fast thickening of oxide scale that is not efficient to release the compressive stress generated from the ZnO/Cu-Zn interfacial reaction Thus, the stress in such thick oxide scale is released by cracking and surface spallation rather than by oxide nanowire growth.

V. CONCLUSIONS

The mechanism underlying the spontaneous ZnO nanowire formation during the oxidation of Cu-Zn has been investigated by a combination of *in situ* XRD and *ex situ* electron microscopy analysis. The oxidation at the temperature ranging from 300 to 600 °C results in the growth of a single ZnO layer and ZnO nanowires on top. Formation of ZnO nanowires is gradually suppressed by increasing the oxidation temperature and correspondingly increased thickness of the underlying ZnO layer. The correlation between the decreased surface density of ZnO nanowires and the increased thickness of the underlying ZnO layer with increasing the oxidation temperature provides a strong evidence that the formation of ZnO nanowire is driven by a stress-driven mechanism. The formation of ZnO nanowires involves generation of compressive stress from the ZnO/Cu-Zn interfacial transformation and relaxation of the compressive stress by outward grain-boundary diffusion of Zn. At lower temperature (~300 °C), relaxation of the compressive stress generated from the interfacial reaction promotes ZnO nanowire growth due to the thin thickness of the ZnO layer while for the oxidation at 500 °C and above the compressive stress is released by oxide cracking and spallation as well as lattice diffusion of Zn, which eliminates the driving force for ZnO nanowire formation.

[1]Z. L. Wang, ACS Nano **2**, 1987–1992 (2008).
[2]X. Wang, J. Song, and Z. L. Wang, J. Mater. Chem. **17**, 711 (2007).
[3]X. Wen, Y. Fang, Q. Pang, C. Yang, J. Wang, W. Ge, K. S. Wong, and S. Yang, J. Phys. Chem. B **109**, 15303–15308 (2005).
[4]H. Wan and H. E. Ruda, J. Mater. Sci: Mater. Electron. **21**, 1014–1019 (2010).
[5]D. Chu, Y. Masuda, T. Ohji, and K. Kato, Langmuir **26**, 2811–2815 (2010).
[6]H. Yu, Z. Zhang, M. Han, X. Hao, and F. Zhu, J. Am. Chem. Soc. **127**, 2378–2379 (2005).
[7]P. X. Gao and Z. L. Wang, Small **1**, 945–949 (2005).
[8]Y. Ding, X. Y. Kong, and Z. L. Wang, Phys. Rev. B **70**, 235408 (2004).
[9]T. Zhai, X. Fang, M. Liao, X. Xu, H. Zeng, B. Yoshio, and D. Golberg, Sensors **9**, 6504–6529 (2009).
[10]E. Comini, C. Baratto, G. Faglia, M. Ferroni, A. Vomiero, and G. Sberveglieri, Prog. Mater. Sci. **54**, 1–67 (2009).
[11]I. Avramov, Nanoscale Res. Lett. **2**, 235–239 (2007).
[12]J. G. Lu, P. Chang, and Z. Fan, Mater. Sci. Eng. R **52**, 49–91 (2006).
[13]N. S. Ramgir, K. Subannajui, Y. Yang, R. Grimm, R. Michiels, and M. Zacharias, J. Phys. Chem. C **114**, 10323–10329 (2010).

[14]E. C. Greyson, Y. Babayan, and T. W. Odom, Adv. Mater. **16**, 1348–1352 (2004).

[15]H. J. Fan, A. S. Barnard, and M. Zacharias, Appl. Phys. Lett. **90**, 143116 (2007).

[16]H. Y. Dang, J. Wang, and S. S. Fan, Nanotechnology **14**, 738–741 (2003).

[17]L.-C. Chao, C.-F. Lin, and C.-C. Liau, Vacuum **86**, 295–298 (2011).

[18]O. Martínez, V. Hortelano, J. Jiménez, J. L. Plaza, S. de Dios, J. Olvera, E. Diéguez, R. Fath, J. G. Lozano, T. Ben, D. González, and J. Mass, J. Alloys Compd. **509**, 5400–5407 (2011).

[19]G.-H. Lee, Electron. Mater. Lett. **6**, 155–159 (2010).

[20]D. C. Kim, B. H. Kong, H. K. Cho, D. J. Park, and J. Y. Lee, Nanotechnology **18**, 015603 (2007).

[21]H.-C. Hsu, Y.-K. Tseng, H.-M. Cheng, J.-H. Kuo, and W.-F. Hsieh, J. Cryst. Growth **261**, 520–525 (2004).

[22]H. Kaifu, H. Yemin, F. Jijiang, W. Xuebin, C. Paul, K. H. Zheng, and C. Yi, J. Phys. Chem. C **111**, 5876–5881 (2007).

[23]C. H. Xu, Z. B. Zhu, H. F. Lui, C. Surya, and S. Q. Shi, Superlattices Microstruct. **49**, 408–415 (2011).

[24]Y. Zhu, C. H. Sow, T. Yu, Q. Zhao, P. Li, Z. Shen, D. Yu, and J. T. L. Thong, Adv. Funct. Mater. **16**, 2415–2422 (2006).

[25]H. Okamoto, *Desk Handbook: Phase Diagrams for Binary Alloys* (ASM International, Materials park, OH, 2000).

[26]H.-Q. Liang, L.-Z. Pan, and Z.-J. Liu, Mater. Lett. **62**, 1797–1800 (2008).

[27]F. Fang, D. X. Zhao, J. Y. Zhang, D. Z. Shen, Y. M. Lu, X. W. Fan, B. H. Li, and X. H. Wang, Mater. Lett. **62**, 1092–1095 (2008).

[28]S. Ren, Y. F. Bai, J. Chen, S. Z. Deng, N. S. Xu, Q. B. Wu, and S. Yang, Mater. Lett. **61**, 666–670 (2007).

[29]A. Bayer, J. Mater. Eng. Perform. **6**, 149–152 (1997).

[30]P. Turchi, M. Sluiter, F. Pinski, D. Johnson, D. Nicholson, G. Stocks, and J. Staunton, Phys. Rev. Lett. **67**, 1779–1782 (1991).

[31]U. Diebold, L. V. Koplitz, and O. Dulub, Appl. Surf. Sci. **237**, 336–342 (2004).

[32]N. Birks, G. H. Meier, and F. S. Pettit, *Introduction to the High Temperature Oxidation of Metals* (Cambridge University Press, 2006).

[33]L. Yuan, Y. Wang, R. Cai, Q. Jiang, J. Wang, B. Li, A. Sharma, and G. Zhou, Mater. Sci. Eng. B **177**, 327–336 (2012).

[34]L. Yuan, Q. Jiang, J. Wang, and G. Zhou, J. Mater. Res. **27**, 1014–1021 (2012).

[35]L. Yuan, Y. Q. Wang, R. Mema, and G. W. Zhou, Acta Mater. **59**, 2491–2500 (2011).

[36]R. Mema, L. Yuan, Q. T. Du, Y. Q. Wang, and G. W. Zhou, Chem. Phys. Lett. **512**, 87–91 (2011).

[37]F. Gao, S. Wang, F. Gesmundo, and Y. Niu, Oxid. Met. **69**, 287–297 (2008).